North Carolina Agricultural and Technical State University

# Aggie Digital Collections and Scholarship

2014

# Improved Weight Functions Of High-Order Weno Schemes

Lee R. Redfearn
*North Carolina Agricultural and Technical State University*

Follow this and additional works at: https://digital.library.ncat.edu/theses

Improved Weight Functions of High-order WENO Schemes

Lee R. Redfearn

North Carolina A&T State University

A thesis submitted to the graduate faculty

in partial fulfillment of the requirements for the degree of

MASTER OF SCIENCE

Department: Mathematics

Major: Applied Mathemaics

Major Professor: Dr. Nail Yamaleev

Greensboro, North Carolina

2014

The Graduate School
North Carolina Agricultural and Technical State University
This is to certify that the Master's Thesis of


Lee R. Redfearn


has met the thesis requirements of
North Carolina Agricultural and Technical State University

Greensboro, North Carolina
2014

Approved by:

_____           _____
Dr. Nail Yamaleev                          Dr. Alexandra Kurepa
Major Professor                            Committee Member


_____           _____
Dr. Guoqing Tang                           Dr. Yevgeniy Rastigeyev
Department Chair                           Committee Member


_____
Dr. Sanjiv Sarin
Dean, The Graduate School

Biographical Sketch

Lee R. Redfearn obtained his Bachelors of Science degree in Pure Mathematics from North Carolina A&T State University in 2012. While pursuing his Masters of science degree in Applied Mathematics, Lee R. Redfearn served as a teacher assistant and tutor for the Department of Mathematics. During his last year, Lee R. Redfearn served as a research assistant to Dr. Yamaleev of the Mathematics Department, aiding in research funded by NASA through the Center of Aviation Safety(CAS). Lee R. Redfearn is a member of the Pi Mu Epsilon National Mathematical Honor Society, as well as the Beta Kappa Chi National Science Honor Society. Upon obtaining his Masters of Science degree, Lee R. Redfearn intends to pursue a doctoral degree in applied mathematics.

## Dedication

For my mother and father. Let this work serve as reverence, for everything that you have given me.

## Acknowledgements

Table of Contents

## List of Figures

Abstract

It has been shown that the conventional 5th-order Weighted Essentially Non-Oscillatory (WENO) scheme of Jiang and Shu degenerates to third order at points where the first and higher order derivatives of the solution become equal to zero. Recently, Yamaleev and Carpenter proposed new weight functions which drastically improve the accuracy of high-order WENO-type schemes and provide the design order of accuracy for smooth solutions with any number of vanishing derivatives, if their tuning parameters satisfy consistency constraints. The truncation error analysis reveals that the accuracy of the flux reconstruction provided by the new weight functions can be increased near strong discontinuities, thus improving the shock-capturing capabilities of the corresponding WENO scheme. Six different modifications of the weight functions of Yamaleev and Carpenter are proposed and analyzed for both smooth and discontinuous solutions. Our grid refinement studies for the linear advection equation show that the modified weight functions improve the non-oscillatory properties of the scheme, while retaining the intended design order of accuracy.

# CHAPTER 1

## Introduction

Weighted Essentially Non-Oscillatory(WENO) schemes have been widely used to simulate physical phenomena involving turbulent flows and shock-turbulence interactions. The conservation laws that govern these physical interactions permit the existence of discontinuous solutions. Approximating such solutions using high-order numerical schemes for problems containing discontinuities or unresolved features leads to oscillatory behavior, known as the Gibbs phenomenon. These spurious oscillations result in the accumulation of error, and in some cases may lead to local or even global instabilities.

WENO methods are derived from the ENO schemes(Essentially non-oscillatory) proposed by Harten et al. [1]. The idea of ENO schemes is to divide a collection of nodes, referred to as a stencil, into smaller candidate stencils. A single candidate stencil is then selected based on a measure of smoothness relative to all candidate stencils. Using this adaptive stencil scheme allows one to avoid passing a polynomial interpolant across a discontinuity, and thereby avoiding spurious oscillations. One of the main drawbacks of the ENO scheme becomes apparent when we consider a problem in which no discontinuities are present. Since each candidate stencil has nearly the same relative measure of smoothness, any small perturbation in the solution triggers the stencil biasing mechanism. In addition, using a single candidate stencil limits the potential accuracy of the approximation because only $r$ points out of $2r$ available points are used for the discretization. The central idea of the WENO scheme, originally developed by Lui and Osher [5] , is to use a linear combination of all low-order fluxes constructed from each candidate stencil to obtain a higher order approximation to the solution. A weight is assigned to each low-order flux, which determines its contribution to the overall approximation. This approach allows for more information to be used in obtaining a higher order approximation, while emulating the adaptive stencil concept of the ENO scheme.

The success of the WENO scheme depends on the measure of smoothness, and the design of the nonlinear weight functions. The weights must be constructed to guarantee convergence to the optimal upwind scheme in smooth regions, while providing non-oscillatory behavior in regions containing discontinuities. The value of each weight is primarily determined by the relative smoothness of the corresponding candidate stencil. For an ENO scheme based on r candidate stencils the highest order that can be achieved is $(r+1)$. A new measure of smoothness presented by Jiang and Shu makes it possible to obtain an $(2r-1)$th order WENO scheme by using a convex combination of local approximations obtained from $r$ candidate stencils.

It was recently shown by Henrick et al. [2] that the classical 5th-order WENO scheme of Jiang and Shu degenerates in accuracy at critical points for smooth solutions. More specifically, the classical 5th-order WENO scheme of Jiang and Shu locally degenerates to 3rd order accuracy. To recover the intended design order of accuracy at critical points while minimizing oscillatory behavior, Henrick et al. developed a mapping for the nonlinear weights. It should be noted that this mapping provides the design order of accuracy only for solutions with a single vanishing derivative. Another approach was proposed by Borges et al. [6]. The main idea of this approach is to solve the problem by developing new weight functions that include a new smoothness indicator of higher order than that of the traditional smoothness indicator of Jiang and Shu. Note however, that these weight functions provide the design order of accuracy only for solutions containing at most two vanishing derivatives. Thus, the retention of design order of accuracy at critical points needed to be generalized to any number of vanishing derivatives.

Recently, a new class of Energy Stable WENO schemes that overcome this degeneration in accuracy has been presented in [8]. ESWENO schemes add and additional artificial dissipation term to prevent local instabilities, in addition to using the WENO reconstruction step with newly defined weight functions. The new weight functions developed in [8] provide reduction of spurious oscillations near discontinuities as well as retain the intended design order of accuracy for any number of vanishing derivatives. This was in part due to the redefining of the second smoothness indicator developed by Borges. The smoothness indicator of Borges, defined as the absolute value

of the difference of smoothness indicators, can not be generalized to the order higher than 5. The second smoothness indicator developed by Yamaleev and Carpenter is based on the highest order Newton's undivided differences involving nodes of the entire stencil.

Examination of the ESWENO scheme shows there is potential to reduce spurious oscillations that occur near strong discontinuities. The main goals of the present work is to optimize the non-oscillatory properties of the ESWENO scheme while retaining the intended design order of accuracy.

The thesis is organized as follows. In Section 2, we give a description of the continuous equation and its discrete counterpart. In Section 3, we describe the conventional WENO scheme of Jiang and Shu. We also present the necessary and sufficient conditions for the nonlinear weight functions, and the new WENO scheme developed by Yamaleev and Carpenter along with its analysis. In Section 4, we present the general analysis and development for the optimized WENO scheme. Numerical results and discussion of the newly optimized WENO scheme are presented in Section 5. Finally in section 6 we summarize our main findings of this work.

## 1.1 Problem Setting; Linear Advection Equation

In this work, we consider the linear advection equation which is given by

$$\frac{\partial u}{\partial t} + \frac{\partial f}{\partial x} = 0, \quad f = au, \quad t \geq 0, \quad 0 \leq x \leq 1,$$

$$u(x,0) = u_0(x) \tag{1.1}$$

It is assumed that the solution is periodic on the domain $0 \leq x \leq 1$ for simplicity. To approximate the solution $u(x,t)$ for a given time $t$, we generate a computational grid by dividing the domain into $N$ intervals with uniform grid spacing $\Delta x = \frac{1}{N}$. The solution $u(x,t)$ for a given time time $t$, is found at each $x_j$th node by approximating the spatial derivative of the flux. To show this, we rewrite (1.1) in the form

$$\frac{\partial u_j}{\partial t} = -\left.\frac{\partial f}{\partial x}\right|_{x=x_j} \tag{1.2}$$

Ideally, we want the finite difference of some function to exactly approximate the spatial derivative of the flux at each node of the computational grid. It is possible to construct such a function implicitly. We define the numerical flux function as follows:

$$f(x) = \frac{1}{\Delta x} \int_{x-\frac{\Delta x}{2}}^{x+\frac{\Delta x}{2}} h(\xi) d\xi.$$  (1.3)

Substituting (1.3) into (1.2) gives us

$$\frac{\partial u_j}{\partial t} = -\left( \frac{h_{j+\frac{1}{2}} - h_{j-\frac{1}{2}}}{\Delta x} \right).$$  (1.4)

Note the numerical function is evaluated at $x_{j\pm\frac{1}{2}} = x_j \pm \frac{\Delta x}{2}$, which will be referred to as the cell boundaries with $x_j$ being the center of each cell. As follows from (1.4), the numerical flux function satisfies the spatial derivative exactly at each node. It is important to remember that our numerical flux function satisfies the spatial derivative exactly only at the grid nodes, and not for each point within the domain. Therefore, our definition of the numerical flux function is itself an approximation to the actual flux function. Since the numerical flux function is not directly obtainable, we must construct flux values $\hat{f}_{j\pm\frac{1}{2}}$ which approximate the values $h_{j\pm\frac{1}{2}}$. By replacing the spatial derivative at each node with a finite difference composed of the approximate values of the numerical flux at the cell boundaries, we now have

$$\frac{\partial u_j}{\partial t} \approx -\left( \frac{\hat{f}_{j+\frac{1}{2}} - \hat{f}_{j-\frac{1}{2}}}{\Delta x} \right).$$  (1.5)

This gives us a system of linear equations that can be solved to obtain an approximation of the entire solution. To construct higher-order approximations of the flux at the cell boundaries, we use a linear combination of low-order flux interpolants constructed from flux values available in a given stencil. So, the spatial derivative is approximated at each node to the $p$th-order of accuracy.

**1.1.1 Continuous analysis.** Let us show that the continuous governing equation (1.1) is conservative and stable in the energy sense. To show the equation is conservative, we integrate

(1.1) across the entire domain $[a, b]$

$$\int_a^b \left( \frac{\partial u}{\partial t} + \frac{\partial f}{\partial x} \right) dx = 0$$

$$\frac{\partial}{\partial t} \int_a^b u dx + \int_a^b \frac{\partial f}{\partial x} dx = 0$$

$$\frac{\partial}{\partial t} \int_a^b u dx + f(b) - f(a) = 0$$

$$\frac{\partial}{\partial t} \int_a^b u dx = f(a) - f(b). \tag{1.6}$$

Therefore, change in the integral of the solution over the entire domain may occur only due to the flux values at the boundaries. Suppose we have the singular perturbed wave equation, subject to the periodic boundary conditions:

$$\frac{\partial u}{\partial t} + \frac{\partial f}{\partial x} = \frac{\partial}{\partial x} \left( B \frac{\partial u}{\partial x} \right), \tag{1.7}$$

with $B$ defined as a nonlinear positive semidefinite differential operator that depends only on $u$ and its derivatives. The term on the right hand side of (1.7) mimics the dissipation operator of the finite difference scheme. It is assumed that (1.7) is subject to the same initial condition as in (1.1). Multiplying by $u$ and integrating across the entire domain gives us

$$\frac{1}{2} \frac{d}{dt} \|u\|_2^2 + \frac{1}{2} au^2 \Big|_0^1 = uBu_x \Big|_0^1 - \int_0^1 u_x Bu_x dx \tag{1.8}$$

Note that the right hand side of the equation is obtained using integration by parts. Knowing that we have periodic boundary conditions and the $B$ is a positive semidefinite operator, we have that

$$\frac{d}{dt} \|u\|_2 = -2 \int_0^1 u_x Bu_x dx \leq 0 \tag{1.9}$$

Equation (1.9) shows that the $L_2$ norm of the solution does not increase in time, thus indicating the continuous problem is stable in the energy sense. Note that if $B = 0$, then the solution is neutrally stable.

**1.1.2 Discrete analysis.** According to [3], if the discrete operator satisfies the summation by parts property, then it follows that the corresponding numerical scheme is stable in the $L_2$-energy

norm. This means the energy expression of the numerical scheme will be negative, or dissipative. We will now show that these properties are retained in the discrete equation. To show conservation, we sum the above discrete equation across the entire computational grid of $J$ nodes. Letting $\Delta x = \frac{1}{J}$, we have

$$\sum_{j=0}^{J} \left[ \frac{\partial u_j}{\partial t} + \frac{f_{j+\frac{1}{2}} - f_{j-\frac{1}{2}}}{\Delta x} \right] \Delta x = 0$$

$$\frac{\partial}{\partial t} \sum_{j=0}^{J} u_j \Delta x + \sum_{j=0}^{J} \left[ \frac{f_{j+\frac{1}{2}} - f_{j-\frac{1}{2}}}{\Delta x} \right] \Delta x = 0$$

$$\frac{\partial}{\partial t} \sum_{j=0}^{J} u_j \Delta x + \left( f_{J+\frac{1}{2}} - f_{-\frac{1}{2}} \right) = 0$$

$$\frac{\partial}{\partial t} \sum_{j=0}^{J} u_j \Delta x = f_{-\frac{1}{2}} - f_{J+\frac{1}{2}} \tag{1.10}$$

Equation (1.1.2) shows that the integral of the solution over the computational domain changes due to the difference of fluxes at the boundaries. Hence the conservative properties of the continuous equation are preserved by the numerical scheme. We now derive a discrete form of the numerical scheme that satisfies the summation by parts property, and show that it is stable in the energy sense. Our discrete approximation of the flux derivative used in (1.1.2) can also be recast in the following form:

$$\frac{\partial \mathbf{f}}{\partial x} = (D_c + D_a) + O(\Delta x^p), \tag{1.11}$$

with $D_c$ being a nonlinear central difference operator defined as

$$D_c = P^{-1} Q; \bar{\mathbf{f}}_x - P^{-1} Q \bar{\mathbf{f}} = O(\Delta x^p),$$

$$P = \Delta x I; Q + Q^T = 0$$

$$\tag{1.12}$$

Note that $D_c$ constructed this way satisfies the summation by parts property. $D_a$ is a nonlinear artificial dissipation term on the right hand side of (1.7). $D_a$ is given as

$$D_a = P^{-1}D_1^T SD_1; \quad P^{-1}D_1^T SD_1\mathbf{u} = O(\Delta x^p); \quad \mathbf{v}^T\left(S+S^T\right)\mathbf{v} \geq 0 \tag{1.13}$$

where $D_1$ is the first-order backward operator, and $P$ is the same positive definite diagonal matrix used in (1.1.2). Using the $D_c$ and $D_a$ operators, (1.7) is discretized as follows:

$$\frac{\partial \mathbf{u}}{\partial t} + P^{-1}Qf = -P^{-1}D_1^T SD_1\mathbf{f}, \tag{1.14}$$

where $\mathbf{f} = a\mathbf{u}$. Multiplying through by $\mathbf{u}^T P$ gives

$$\frac{d}{dt}\|u\|_P^2 + a\mathbf{u}^T Q\mathbf{u} = -a\left(D_1\mathbf{u}\right)^T SD_1\mathbf{u} \tag{1.15}$$

adding this equation to its transpose yields

$$\frac{d}{dt}\|u\|_P^2 + a\mathbf{u}^T\left(Q+Q^T\right)\mathbf{u} = -a\left(D_1\mathbf{u}\right)^T\left(S+S^T\right)D_1\mathbf{u} \tag{1.16}$$

Because $Q$ is skew-symmetric and $S$ is positive semi-definite, we have that

$$\frac{d}{dt}\|u\|_P^2 = -a\left(D_1\mathbf{u}\right)^T\left(S+S^T\right)D_1\mathbf{u} \leq 0 \tag{1.17}$$

As follows from (1.17), the numerical scheme is stable in the energy norm.

# CHAPTER 2

## Literature Review

Linear schemes have been widely used to solve partial differential equations such as (1.1). A linear scheme is one in which each term in the approximation has a fixed coefficient, or contribution, for all nodes on the computational grid. However, using a linear scheme to approximate discontinuous solutions results in the Gibbs phenomenon, which is characterized by the occurrence of oscillations. Weighted Essentially Non-Oscillatory (WENO) schemes are preferred in such cases because they are nonlinear schemes, that is, each contribution in the approximation is weighted based on the solution smoothness which detects the presence of discontinuities near the contributing stencil. This mimics the stencil biasing property of the ENO scheme [1] to avoid oscillatory behavior, and uses the smoothest information available to achieve good shock-capturing capabilities.

## 2.1 Conventional 5th-order WENO Schemes

We now look to approximate the solution of the linear advection equation at each node using the conventional 5th-order WENO scheme of Jiang and Shu. The approximation at each node is a finite difference scheme constructed from higher-order fluxes evaluated at the cell boundaries. These fluxes are defined as

$$\hat{f}_{j\pm\frac{1}{2}} = \sum_r \omega^{(r)}_{j\pm\frac{1}{2}} f^{(r)}_{j\pm\frac{1}{2}}, \tag{2.1}$$

where each $f^{(r)}_{j\pm\frac{1}{2}}$ is a third-order reconstruction of the flux from the candidate stencil, along with its corresponding weight $\omega^{(r)}_{j\pm\frac{1}{2}}$. Our third-order fluxes are defined as

$$
\begin{pmatrix}
f^{LL}\left(u_{j+\frac{1}{2}}\right) \\
f^{L}(u_{j+\frac{1}{2}}) \\
f^{R}(u_{j+\frac{1}{2}}) \\
f^{RR}(u_{j+\frac{1}{2}})
\end{pmatrix}
=
\begin{pmatrix}
2 & -7 & 11 & 0 & 0 & 0 \\
0 & -1 & 5 & 2 & 0 & 0 \\
0 & 0 & 2 & 5 & -1 & 0 \\
0 & 0 & 0 & 0 & 11 & -7
\end{pmatrix}
\begin{pmatrix}
f\left(u_{j-2}\right) \\
f\left(u_{j-1}\right) \\
f\left(u_{j}\right) \\
f\left(u_{j+1}\right) \\
f\left(u_{j+2}\right) \\
f\left(u_{j+3}\right)
\end{pmatrix},
\tag{2.2}
$$

The addition of the stencil $S_{RR}$ makes the entire WENO reconstruction stencil symmetric with respect to the $x_{j\pm\frac{1}{2}}$th point. As has been shown in [8], this additional candidate stencil allows us to increase the design order of the conventional 5th-order WENO scheme of Jiang and Shu by one, thus making it 6th-order accurate. Work concerning the stability development of this 6th-order scheme is presented in [8]. The weight functions of the conventional 5th-order WENO scheme are given as follows:

$$
\omega^{(r)}_{j\pm\frac{1}{2}} = \frac{\alpha_r}{\sum_r \alpha_r}, \qquad \alpha_r = \frac{d^{(r)}}{\left(\varepsilon + \beta^{(r)}\right)^2},
\tag{2.3}
$$

where $\alpha_r$ is an unnormalized weight, and $d^{(r)}$ is an ideal weight. Using each $d^{(r)}$ as a weight results in the linear upwind scheme. Each candidate stencil has a smoothness indicator defined as:

$$
\beta^{(r)} = \sum_{l=1}^{s-1} \Delta x^{2l-1} \int_{x_{j-\frac{1}{2}}}^{x_{j+\frac{1}{2}}} \left(\frac{d^l q_r(x)}{dx^l}\right)^2 dx
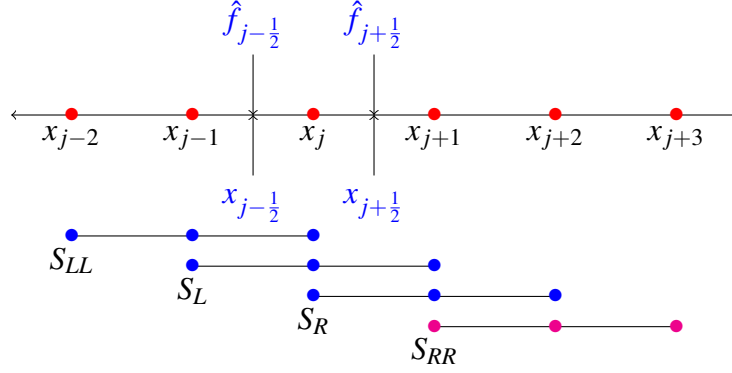\tag{2.4}
$$

*Figure 1.* Stencil of WENO Flux Reconstruction; the stencil $S_{RR}$ is used to obtain a 6th order scheme. Each $S_r$ has a measure of smoothness, $\beta^{(r)}$.

We can express the smoothness indicators with respect to nodal flux values as follows:

$$
\begin{aligned}
\beta^{LL} &= \tfrac{13}{12}\left(f_{j-2}-2f_{j-1}+f_j\right)^2 + \tfrac{1}{4}\left(f_{j-2}-4f_{j-1}+3f_j\right)^2 \\
\beta^{L} &= \tfrac{13}{12}\left(f_{j-1}-2f_j+f_{j+1}\right)^2 + \tfrac{1}{4}\left(f_{j-1}-f_{j+1}\right)^2 \\
\beta^{R} &= \tfrac{13}{12}\left(f_j-2f_{j+1}+f_{j+2}\right)^2 + \tfrac{1}{4}\left(3f_j-4f_{j+1}+f_{j+2}\right)^2 \\
\beta^{RR} &= \tfrac{13}{12}\left(f_{j+1}-2f_{j+2}+f_{j+3}\right)^2 + \tfrac{1}{4}\left(-5f_{j+1}+8f_{j+2}-3f_{j+3}\right)^2
\end{aligned}
\tag{2.5}
$$

From examination of the conventional weights we see that in smooth flow regions, the weight functions $w^{(r)}$ approach their target values $d^{(r)}$. Note however, that near a strong discontinuity, the weight function associated with the stencil containing the shock is effectively nullified, thus biasing the stencil away from the strong discontinuity.

### 2.1.1 Consistency of the WENO scheme.

It is well known that the conventional WENO scheme is overly dissipative. In [2], it has been shown that at points where the first derivative vanishes, the conventional 5th-order WENO scheme of Jiang and Shu degenerates to 3rd-order accuracy. As shown in [4], a sufficient condition on the nonlinear weights to provide 5th-order accuracy is

$$
\omega^{(r)}_{j\pm\frac{1}{2}} = d^{(r)} + O(\Delta x^2)
\tag{2.6}
$$

We now demonstrate that a stricter condition should be imposed on the nonlinear weights of the 5th-order WENO scheme to retain design order of accuracy for any number of vanishing derivatives. Here we derive the necessary and sufficient conditions for the nonlinear weights of any WENO-type scheme to provide $p$th-order accuracy. The approach is to compare the $p$th-order accurate nonlinear and linear scheme, and establish a relationship between the set of nonlinear weights $\{\omega_{j\pm\frac{1}{2}}^{(r)}\}$ and the set of linear ideal weights $\{d^{(r)}\}$. A WENO-type scheme can be written in the following form

$$\left[D^{WENO}f\right]_j = \frac{\hat{f}_{j+\frac{1}{2}} - \hat{f}_{j-\frac{1}{2}}}{\Delta x} = \frac{\partial f}{\partial x}\big|_{x=x_j} + O(\Delta x^p). \tag{2.7}$$

For sufficiently smooth solutions, we use the ideal weights which correspond to the upwind scheme to approximate the flux. This differential operator is given as

$$\left[D^{IDEAL}f\right]_j = \frac{\hat{f}^*_{j+\frac{1}{2}} - \hat{f}^*_{j-\frac{1}{2}}}{\Delta x} = \frac{\partial f}{\partial x}\big|_{x=x_j} + O(\Delta x^p). \tag{2.8}$$

Subtracting the linear scheme from the nonlinear scheme gives us

$$\left[D^{WENO}f\right]_j - \left[D^{IDEAL}f\right]_j = \frac{\sum_r\left[\left(\omega_{j+\frac{1}{2}}^{(r)} - d^{(r)}\right)f_{j+\frac{1}{2}}^{(r)} - \left(\omega_{j-\frac{1}{2}}^{(r)} - d^{(r)}\right)f_{j-\frac{1}{2}}^{(r)}\right]}{\Delta x}$$

$$= \frac{1}{\Delta x}\sum_r\left[\left(\omega_{j+\frac{1}{2}}^{(r)} - d^{(r)}\right)h\left(x_{j+\frac{1}{2}}\right) - \left(\omega_{j-\frac{1}{2}}^{(r)} - d^{(r)}\right)h\left(x_{j-\frac{1}{2}}\right)\right]$$

$$+ \sum_{l=s}^{p}\sum_r \Delta x^{l-1}c_l^{(r)}\left[\left(\omega_{j+\frac{1}{2}}^{(r)} - d^{(r)}\right) - \left(\omega_{j-\frac{1}{2}}^{(r)} - d^{(r)}\right)\right] + O(\Delta x^p). \tag{2.9}$$

Examining each term in this expression, we obtain the following necessary conditions:

$$\sum_r\left[w_{j\pm\frac{1}{2}}^{(r)} - d^{(r)}\right] = O(\Delta x^{p+1})$$

$$\sum_r\left[\left(w_{j+\frac{1}{2}}^{(r)} - d^{(r)}\right) - \left(w_{j-\frac{1}{2}}^{(r)} - d^{(r)}\right)\right] = O(\Delta x)$$

$$\sum_r\left[\left(w_{j+\frac{1}{2}}^{(r)} - d^{(r)}\right) - \left(w_{j-\frac{1}{2}}^{(r)} - d^{(r)}\right)\right] = O(\Delta x^{p-s+1}) \tag{2.10}$$

The first condition in (2.1.1) is always satisfied because of the normalization of the weight functions and target values. The remaining conditions are met if the following sufficient condition is imposed on the weights:

$$\omega_{j\pm\frac{1}{2}}^{(r)} - d^{(r)} = O(\Delta x^{p-s+1}),$$

(2.11)

For the conventional 5th-order WENO scheme, $p$ and $s$ are set equal to 5 and 3, respectively, thus leading to

$$\omega_{j\pm\frac{1}{2}}^{(r)} - d^{(r)} = O(\Delta x^3).$$

(2.12)

As follows from (2.12), stricter constraints than (2.6) should be imposed on the weight functions of the conventional 5th-order WENO schemes.

## 2.2 Energy Stable WENO Scheme.

Based on numerical simulations of turbulent flows, it has been observed that the conventional WENO scheme of Jiang and Shu may become unstable. This observation was proven formally in [8] after Yamaleev and Carpenter examined the symmetric component of the conventional WENO operator, and found that it contains eigenvalues that has a positive real part. From this analysis it follows that the conventional WENO scheme could become locally unstable when approximating the problems with discontinuities or unresolved features. To remedy this, Yamaleev and Carpenter developed the energy stable WENO (ESWENO) scheme by adding an additional artificial dissipative term to the conventional WENO discrete operator. As a result, an energy estimate can be obtained for the modified WENO operator, thus ensuring the stability of the numerical scheme. In addition, Yamaleev and Carpenter derived new formulas for the weight functions which satisfies (2.11) for any number of vanishing derivatives. As a whole, the ESWENO scheme provides satisfactory non-oscillatory behavior near discontinuities while satisfying (2.11) for any number of of vanishing derivatives, hence retaining the design order of accuracy at critical points. The ESWENO scheme retains the same definition of smoothness indicators given in (2.4).

The redefined weight functions are defined as

$$\omega^{(r)} = \frac{\alpha_r}{\sum_l \alpha_l}, \quad \alpha_r = d^{(r)} \left( 1 + \frac{\tau_p}{\epsilon + \beta^{(r)}} \right), \tag{2.13}$$

where $\tau_p$ is the global smoothness indicator. For $p = 5$, $\tau_5$ is given by

$$\tau_5 = \left( -f_{j-2} + 5f_{j-1} - 10f_j + 10f_{j+1} - 5f_{j+2} + f_{j+3} \right)^2. \tag{2.14}$$

The weight functions given by (2.13) are similar to those developed by Borges et al. in [6]. Note, however, that the parameter $\tau_p$ in [6] differs from the global smoothness indicator given by (2.14) and cannot be directly generalized to $p = 6$ or higher.

**2.2.1 Analysis of ESWENO scheme for discontinuous flows.** Let us show that the flux reconstruction based on the weight functions given by (1.14-15) degenerates from 3rd to 2nd order near strong discontinuities. We now demonstrate this loss in accuracy through truncation error analysis. Suppose that we have a discontinuity such that it is contained in the candidate stencils $S_{LL}$ and $S_L$. Expanding the smoothness indicators in Taylor series, we have

$$\tau_p = O(1)$$

$$\beta^{LL} = O(1)$$

$$\beta^L = O(1)$$

$$\beta^R = f'^2 \Delta x^2 + \left( \frac{13}{12} f''^2 - \frac{2}{3} f' f''' \right) \Delta x^4 + \left( \frac{13}{6} f'' f''' - \frac{1}{2} f' f'''' \right) \Delta x^5 + O(\Delta x^6)$$

$$\beta^{RR} = f'^2 \Delta x^2 + \left( \frac{13}{12} f''^2 - \frac{11}{3} f' f''' \right) \Delta x^4 + \left( \frac{13}{3} f'' f''' - 5 f' f'''' \right) \Delta x^5 + O(\Delta x^6). \tag{2.15}$$

As previously stated, the newly designed weights of the ESWENO scheme are just 2nd-order accurate near the strong discontinuity. We now demonstrate this fact. The nonlinear weight

functions take the following form:

$$\omega_{j\pm\frac{1}{2}}^{r=L,LL} = \frac{d^{LL}\left(1+\frac{O(1)}{\varepsilon+O(1)}\right)}{1+\frac{O(1)}{\varepsilon+O(1)}+\sum_{r\neq L,LL}\frac{O(1)}{\varepsilon+O(\Delta x^2)}} = \frac{O(1)}{O(1)+\frac{O(1)}{\varepsilon+O(\Delta x^2)}} = O(1)\left(\varepsilon+O\left(\Delta x^2\right)\right),$$

$$\omega_{j\pm\frac{1}{2}}^{r=R,RR} = \frac{d^{(r)}\left[1+\frac{O(1)}{\varepsilon+O(\Delta x^2)}\right]}{O(1)+\frac{(d^{(r)}+d^{RR})O(1)}{\varepsilon+O(\Delta x^2)}} \approx \frac{d^{(r)}\left(\varepsilon+O(\Delta x^2)+O(1)\right)}{\left(d^R+d^{RR}\right)O(1)} \approx \frac{d^{(r)}}{d^R+d^{RR}}. \tag{2.16}$$

We now attempt to construct the high-order approximation using the weights and the low-order flux functions.

$$\frac{\hat{f}_{j+\frac{1}{2}}-\hat{f}_{j-\frac{1}{2}}}{\Delta x} = \frac{O(\Delta x^2)\sum_{r=L,LL}\left[f_{j+\frac{1}{2}}^{(r)}-f_{j-\frac{1}{2}}^{(r)}\right]+\sum_{r=R,RR}\frac{d^{(r)}}{d^R+d^{RR}}\left[f_{j+\frac{1}{2}}^{(r)}-f_{j-\frac{1}{2}}^{(r)}\right]}{\Delta x}$$
$$\approx \frac{f'+O(\Delta x^2)}{\Delta x} \approx f'+O(\Delta x). \tag{2.17}$$

Here we see that the spatial derivative approximation locally degenerates to only 1st order. We want to improve the local reconstruction order, thus providing improved non-oscillatory behavior and retaining 3rd-order accuracy for the flux reconstruction.

# CHAPTER 3

## Methodology

We want to modify the weight functions of the ESWENO scheme to improve the design order of flux reconstruction for discontinuous solutions. The modification is aimed at improving the non-oscillatory behavior of the ESWENO scheme, while providing design order of accuracy in smooth regions of the solution. Recall that the nonlinear weights are designed to nullify the contribution of fluxes based on stencils containing discontinuities, and converge to the ideal weights of the upwind scheme in smooth regions.

### 3.1  Weight functions of the 5th-order ESWENO scheme

We first examine the existing weights of the ESWENO scheme for accuracy. As shown in [7], the current weights satisfy the necessary and sufficient condition (2.11) for any number of vanishing derivatives. Expanding the weight function in a Taylor series yields

$$\omega_{j\pm\frac{1}{2}}^{(r)} = \frac{d^{(r)}\left(1+\frac{\tau_p}{\varepsilon+\beta^{(r)}}\right)}{1+\sum_k \frac{\tau_p d^{(r)}}{\varepsilon+\beta^{(k)}}} \approx d^{(r)}\left(1+\frac{\tau_p}{\varepsilon+\beta^{(r)}}\right)\left(1-\sum_k \frac{\tau_p d^{(r)}}{\varepsilon+\beta^{(k)}}\right)$$

$$= d^{(r)} + \frac{d^{(r)}\tau_p}{\varepsilon+\beta^{(r)}} - \sum_k \frac{\tau_p d^{(k)}}{\varepsilon+\beta^{(k)}} = d^{(r)} - \sum_{k\neq r} \frac{\tau_p d^{(k)}}{\varepsilon+\beta^{(k)}} + O\left(\left(\frac{\tau_p d^{(r)}}{\varepsilon+\beta^{(k)}}\right)^2\right) \tag{3.1}$$

Using the sufficient condition for consistency (2.11), we have

$$\frac{\tau_p}{\varepsilon+\beta^{(r)}} \leq O(\Delta x^{p-s+1}). \tag{3.2}$$

Equation (3.2) shows that satisfaction of (2.11) will depend on the smoothness indcator terms $\tau_p$ and $\beta^{(r)}$ of the weight functions. The Yamaleev and Carpenter(Y-C) weights of the ESWENO scheme provide non-oscillatory behavior near strong discontinuities, and retention of design order of accuracy for smooth solutions. By making a modification to the Y-C weights we can develop

new set of weights to examine. The new weight functions are defined as follows:

$$\alpha_r = d^{(r)}\left(1 + \frac{\tau_p^k}{\left(\varepsilon + \beta^{(r)}\right)^m}\right).$$

(3.3)

Using (3.3), we can make our new weights satisfy (3.2) by writing

$$\frac{\tau_p^k}{\left(\varepsilon + \beta^{(r)}\right)^m} \le O(\Delta x^{p-s+1}).$$

(3.4)

With the new form of the weight functions, our goal is to find optimum values of $k$ and $m$ such that the numerical solution is free of spurious oscillations on refined grids, while retaining the design order of accuracy in regions where the solution is sufficiently smooth. To derive constraints on the parameters $k$ and $m$, we will use truncation analysis for continuous and discontinuous solutions.

**3.1.1 Constraint of the parameter $\varepsilon$.** First, we derive bounds on $\varepsilon$ to ensure the parameter provides the necessary consistency for the nonlinear weights to converge to the ideal weights. Expanding the new weight functions in a Taylor series yields

$$\alpha_r = d^{(r)}\left(1 + \frac{O(\Delta x^{2pk})}{(\varepsilon + O(\Delta x^2))^m}\right)$$

(3.5)

Due to the necessary and sufficient condition, we must have that

$$\frac{\tau_p^k}{\left(\varepsilon + \beta^{(r)}\right)^m} \le O(\Delta x^{p-s+1})$$

(3.6)

or equivalently

$$\frac{O(\Delta x^{2pk})}{(\varepsilon + O(\Delta x^2))^m} \le O(\Delta x^{p-s+1})$$

(3.7)

Assuming that the solution has several vanishing derivatives so that $\beta_r \approx 0$, we obtain a lower bound on $\varepsilon$

$$\frac{O(\Delta x^{2pk})}{\varepsilon^m} \le O(\Delta x^{p-s+1}),$$

(3.8)

Which leads to

$$O\left(\Delta x^{\frac{2pk-p+s-1}{m}}\right) \leq \varepsilon. \tag{3.9}$$

Since the parameter $\varepsilon$ determines the amplitude of the smallest oscillations detected by the ESWENO scheme, we set $\varepsilon$ to be equal to its lower bound given by (3.9).

## 3.2 Analysis of Improved Weight Functions

### 3.2.1 Continuous solutions.
We perform truncation error analysis for the case when the solution is sufficiently smooth, to infer information about the new parameters. Assume that the solution is $2pk$ times continuously differentiable and continuous, where we also assume that $f' \neq 0$ and $\varepsilon \leq O(\Delta x^2)$. Let $C_r$ be the coefficient in front of the $O(\Delta x^4)$ term of the Taylor series expansion of $\beta^{(r)}$. Then the weight function $w_{LL}$ can be expanded as follows:

$$\omega_{LL} = \frac{d_{LL}\left[1 + \frac{\left(f^{(p)}\right)^{2k}\Delta x^{2pk}}{\left(\varepsilon + (f')^2\Delta x^2 + C_{LL}\Delta x^4\right)^m}\right]}{1 + \sum_r \frac{d_r\left(f^{(p)}\right)^{2k}\Delta x^{2pk}}{\left(\varepsilon + (f')^2\Delta x^2 + C_r\Delta x^4\right)^m}} = \frac{d^{(r)}\left[1 + \frac{\left(f^{(p)}\right)^{2k}\Delta x^{2pk}}{\left(\varepsilon + (f')^2\Delta x^2\right)^m\left[1 + \frac{C_{LL}\Delta x^4}{\varepsilon + (f')^2\Delta x^2}\right]^m}\right]}{1 + \sum_r \frac{d^{(r)}\left(f^{(p)}\right)^2\Delta x^{2pk}}{\left(\varepsilon + (f')^2\Delta x^2\right)^m\left[1 + \frac{C_r\Delta x^4}{\varepsilon + (f')^2\Delta x^2}\right]^m}}. \tag{3.10}$$

Performing further manipulation of this expression, we obtain

$$\omega_{LL} = d_{LL} + \Delta x^{2pk-2m+2}\frac{\left(f^{(p)}\right)^{2k}}{(f')^{2m+1}}\left[C_{LL} - \sum_r C_r d_r\right] \tag{3.11}$$

Substituting these weights in the convex combination of $\hat{f}_{j\pm\frac{1}{2}}$ leads us to

$$\hat{f}_{j\pm\frac{1}{2}} = h_{j\pm\frac{1}{2}} + O\left(\Delta x^{2pk-2m+2}\right). \tag{3.12}$$

From (3.12), we can conclude that in order to retain $p$th-order of accuracy, the parameters $k$ and $m$ should satisfy the following inequality

$$2pk - 2m + 2 \geq p - s + 1. \tag{3.13}$$

**3.2.2  Discontinuous solutions.**  To obtain a complete set of constraints on the parameters $k$ and $m$, we must consider not only smooth solutions, but also discontinuous solutions. Without loss of generality, let us assume a shock or discontinuity, is contained in the candidate stencil $S_{LL}$. The unnormalized weight for this candidate stencil can be written in the following form

$$\alpha_{LL} = d_{LL}\left[1 + \frac{O(1)}{(\varepsilon + O(1))^m}\right]. \tag{3.14}$$

For all other candidate stencils, we have

$$\alpha_{r \neq LL} = d_r\left[1 + \frac{O(1)}{\left(\varepsilon + (f')^2 \Delta x^2\right)}\right]. \tag{3.15}$$

Combining these expressions, we obtain

$$\omega_{LL} = \frac{d_{LL}\left[1 + \frac{O(1)}{(\varepsilon + O(1))^m}\right]}{O(1) + \frac{(d_L + d_R)O(1)}{\left(\varepsilon + (f')^2 \Delta x^2\right)^m}} = O(1)\left(\varepsilon + \left(f'\right)^2 \Delta x^2\right)^m. \tag{3.16}$$

To retain the design order of the reconstruction near a strong discontinuity, the following constraint should be imposed:

$$O(\Delta x^{2m}) \leq O(\Delta x^{p-s+1}). \tag{3.17}$$

For the 5th-order case, this gives us

$$m \geq \frac{3}{2}. \tag{3.18}$$

Because each examined relationship between $m$ and $k$ is linear, we are unable to bound the parameter $k$ without imposing additional constraints on the parameters. This implies that parameters $k$ and $m$ can assume infinitely many values. Using (3.18) and (3.7), we can represent the possible values of the parameters; as shown below in Figure 2.
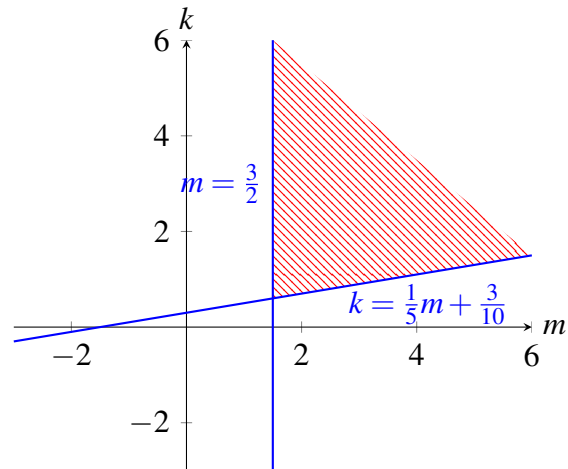
*Figure 2.* Graph of inequalities obtained from truncation error analysis showing the possible values of parameters $k$ and $m$.

We note that as we increase the value of $k$, the rate of convergence increases. However, by increasing the rate of convergence, we also increase the stiffness of the discrete ESWENO operator. To obtain reasonable choices for the parameters we look to compare non-oscillatory behavior and convergence rate of error of numerical solutions, using both the conventional ESWENO weights and the new weights.

# CHAPTER 4

## Results

In the previous section, we developed a new form of the weight functions for the ESWENO scheme to further reduce oscillatory behavior near strong discontinuities. We derived restrictions on the parameters $k$ and $m$ of the new weights, ensuring these functions will provide $p$th-order accuracy for regions where the solution is smooth. We have shown that without any additional assumptions, $k$ and $m$ can assume an infinite number of values, which presents a problem for the discretization of nonlinear solutions. More specifically, as we increase the values of $k$ and $m$, we also increase the stiffness of the numerical scheme. This forces us to select much smaller time steps, which increases the computational cost to obtain a stable numerical solution. For this reason, we choose the values of $k$ and $m$, so that they are close to the lower bound values. The idea is to obtain the desired properties in the new nonlinear weights, without having unnecessarily large values of $k$ and $m$ which increase the stiffness of the numerical scheme. We now conduct numerical experiments with several values of $k$ and $m$. The two values of $m$ that were chosen were m=1.5 and m=2; the former value being the lower bound of $m$, and the latter being a value which is close to the lower bound of $m$. Another reason $m = 2$ was chosen is because in the present literature of WENO schemes this value of $m$ is used to create a difference in scales amongst regions that contain discontinuities, and those where the solution is smooth, Borges et al. [6]. The selected values of $k$ that we will consider are $k = 1.5, 1.75, 2$. Two of these values being the same as $m$, and one being the average of the chosen values of $m$. Each value of $k$ is paired with each value of $m$, and used as the exponents in the improved weight functions. The results obtained using each paired value of $k$ and $m$ will be compared with the results obtained using the weight functions of the ESWENO scheme developed in [8]. We examine reduced non-oscillatory behavior for the discontinuous solution, as well as the convergence rate of error for continuous solutions. For the continuous case, we are looking for convergence with design order of accuracy, and for the discontinuous solution,

we are looking to completely eliminated, or significantly reduce overshoots and undershoots near points of discontinuity.

## 4.1 Error Convergence for Continuous Solution

We know that for a continuous solution, the ideal weights $d^{(r)}$ create a linear scheme whose solution converges with $p$th-order accuracy. Here, we will look to see which values of $k$ and $m$ provide the convergence rate of the linear scheme. We would also like to identify those values of $k$ and $m$ that cause a degradation in the design order of accuracy. If there is a degradation of accuracy, then the value of the parameters which produced this loss in accuracy cannot be considered in the final form of the improved weights of the ESWENO scheme. The functions used in the numerical simulations are those which satisfy (1.1), where we let $a = 1$. For the continuous solution, the function used is $y = e^{-300x^2}$. For the discontinuous solution, we choose the equation which models the propagation of a square pulse. For both the continuous and discontinuous solution we retain periodic boundary conditions on the domain $[0, 1]$, that is $u(0) = u(1)$.
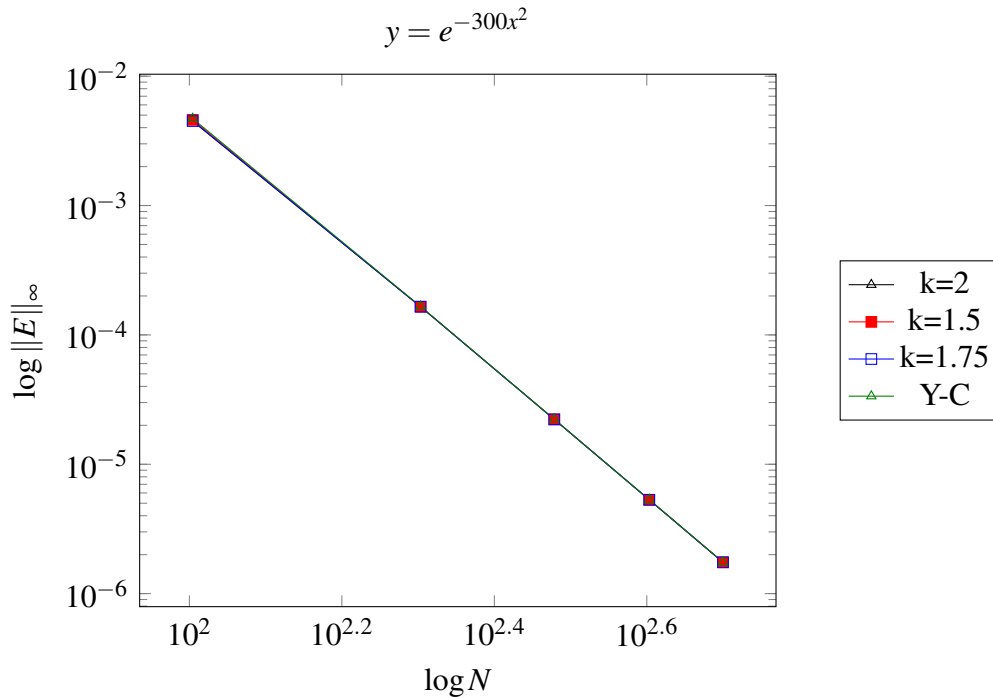


*Figure 3.* Error Convergence of 5th order ESWENO schemes with m=1.5 and selected values of k; k=1 for Y-C.

For the case that $m = 1.5$, the error converges monotonically at the 5th-order rate for all values of $k$, as one can see in Figure 3. These results will be compared with the convergence rate of error when $m = 2$, for all values of $k$.
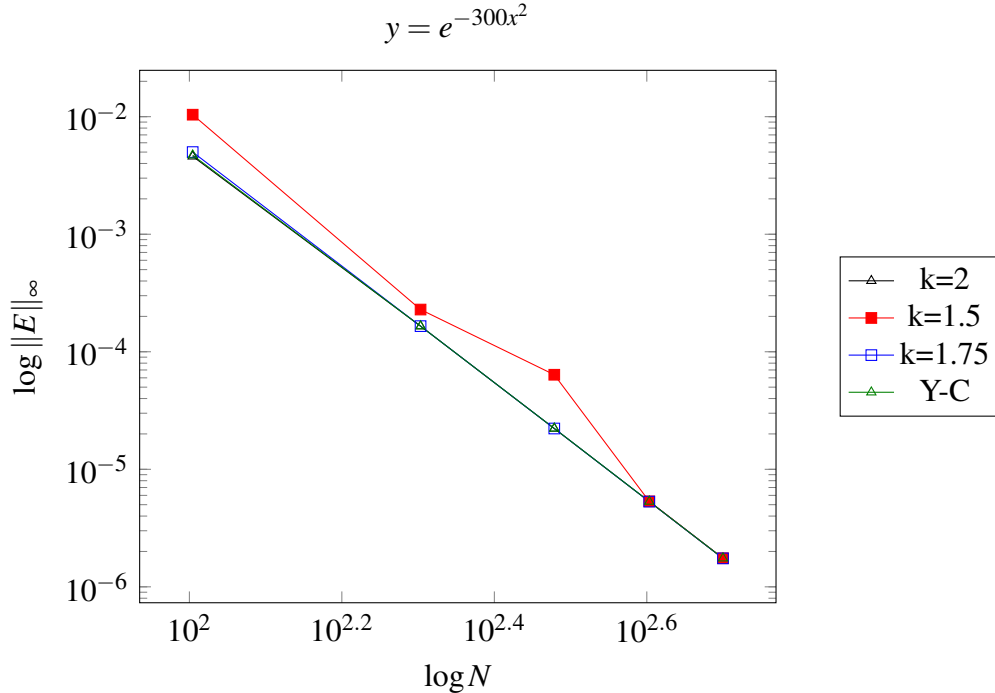


$$y = e^{-300x^2}$$

*Figure 4.* Error convergence of 5th order ESWENO schemes with m=2 and selected values of k; k=1 for Y-C.

When *m* is set equal to 2, we see that the error converges at the 5th-order rate for all values of *k*. However, when $k = 1.5$, the numerical scheme loses accuracy on coarse computational grids. After refining the computational grid, monotonic converge of the error at the 5th-order rate is obtained for all values of *k*. To make conclusive statements concerning values of the parameters *m* and *k*, we will need to analyze the results for problems with strong discontinuities.

## 4.2 Discontinuous Solutions

For problems with discontinuous solutions, we look to improve local non-oscillatory behavior and retain good shock-capturing capabilities of the original ESWENO scheme. The results of each pair of parameter values will be compared with the exact solution of the propagation of a square pulse, as well as the results obtained using the ESWENO scheme with the new weight

functions. Here, we are looking for significant reductions in oscillatory behavior near points of discontinuity.
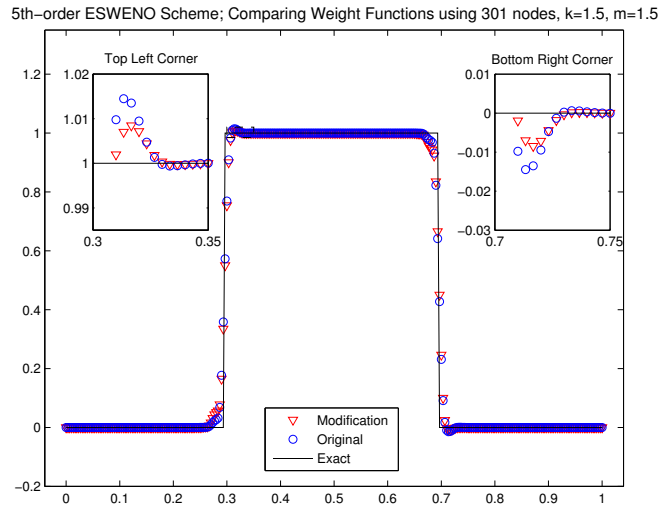


*Figure 5.* The exact and numerical solutions obtained using he ESWENO scheme with
$$k = m = 1.5.$$

As one can see in Figure 5, the new weight functions with $k = m = 1.5$ improve non-oscillatory behavior near discontinuities when compared to the results obtained using the Y-C weight functions of the ESWENO scheme. Despite that the amplitude of overshoots and undershoots near the discontinuities has been reduced by about a factor of two, the numerical solution still exhibits oscillatory behavior.
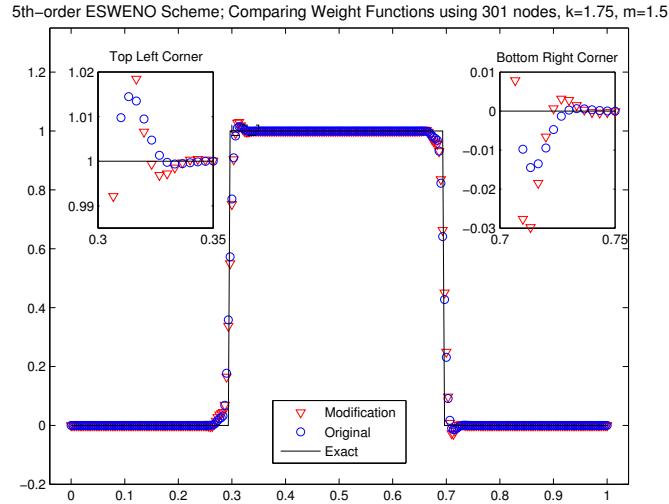
*Figure 6.* The exact and numerical solutions obtained using the ESWENO scheme with $k = 1.75$ and $m = 1.5$.

Though the new weight functions with $k = 1.75$ and $m = 1.5$ provide the 5th order of accuracy for smooth solutions, we see that for these parameter values, oscillatory behavior is magnified near the discontinuities, as seen in Figure 6. Note that $k > m$ in this instance. To make a conclusive statement concerning the increase in the amplitude of oscillations if $k > m$, we have further increased $k$, while keeping $m$ unchanged.
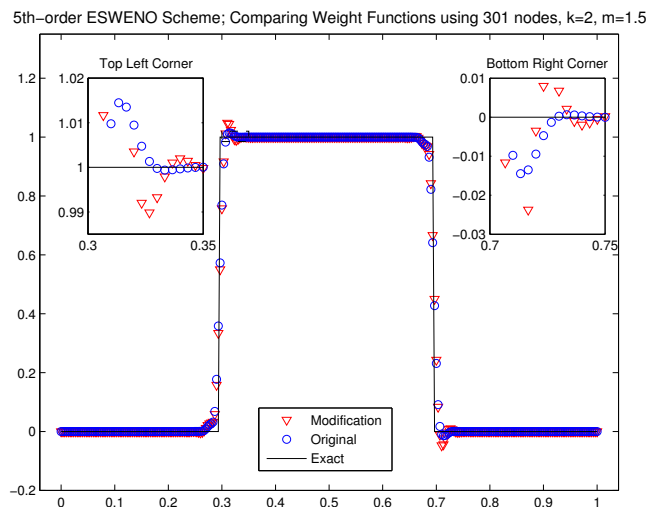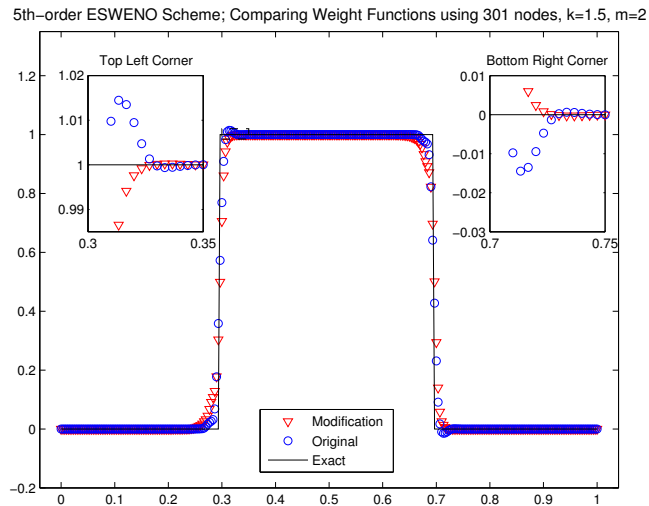


*Figure 7.* The exact and numerical solutions obtained using the ESWENO scheme with $k = 2$ and $m = 1.5$.

Figure 7 shows that oscillatory behavior is amplified, thus underperforming the results of the original weight functions. Regardless of the fact that $m = 1.5$ and $k = 2$ provides 5th-order accuracy for smooth solutions, these parameter values do not provide the reduction in oscillatory behavior.

Based on the results presented above, we see that for $m = 1.5$, oscillations have been damped when the parameters $k$ and $m$ are equal in value. Raising the value of $k$ beyond the value of $m$ results in amplified oscillatory behavior more severe than results produced by the original weight functions. We will now consider a new value of $m$ with the same set of values for $k$. In the next set of results, we let $m = 2$. Originally, m=2 was chosen to create a difference in scales, which is used to identify potential regions containing discontinuities. This implies that raising the power of m deals with the damping factor of oscillations. Here, we follow the guidance of the literature and have $m = 2$ and examine the quality of non-oscillatory behavior of the numerical scheme.



*Figure 8.* The exact and numerical solutions obtained using the ESWENO scheme with $k = 1.5$ and $m = 2$.

Figure 8 shows that the numerical solution is free of spurious oscillations without begin overly dissipative. As compared to the results of the original weight functions, we see that recovering the reconstruction order near discontinuities significantly improves the shock-capturing capabilities of the ESWENO scheme.
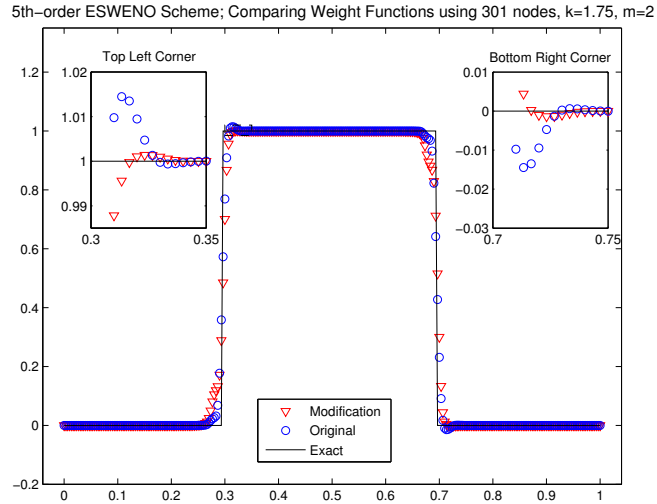
*Figure 9.* The exact and numerical solutions obtained using the ESWENO scheme with $k = 1.75$ and $m = 2$.

The solution profile is nearly monotonic, thus indicating that the new weight functions with $k = 1.75$ and $m = 2$ outperform the original Y-C weights in terms of the damping of oscillations. The results are slightly less effective than those obtained using $m = 2$ and $k = 1.5$.
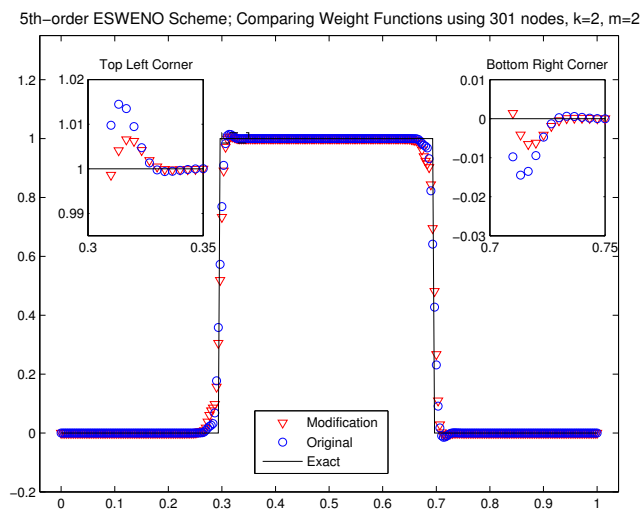


*Figure 10.* The exact and numerical solutions obtained using the ESWENO scheme with $k = 2$ and $m = 2$.

As in the case of $m = 1.5$, we see that the amplitude of oscillation increases as $k$ becomes larger. Having $k = 2$ and $m = 2$ reduces oscillatory behavior near discontinuities, but the results

are less effective than those obtained using $k = 1.75$ and $m = 2$. Results obtained for $k = 2$ show that the solution becomes more oscillatory near the discontinuities. It appears that having $k = 1.5$ provides the best accuracy for the discontinuous solution and the design order of accuracy for smooth solutions.

Choosing the smallest possible values of $k$ and $m$ implies the resulting numerical scheme will produce the desired properties, without unnecessarily increasing the stiffness of the WENO operator. A plot of the error convergence rate is given for the case when $m = 1.5$ and $k = .6$; the smallest possible value of $k$ when $m = 1.5$.
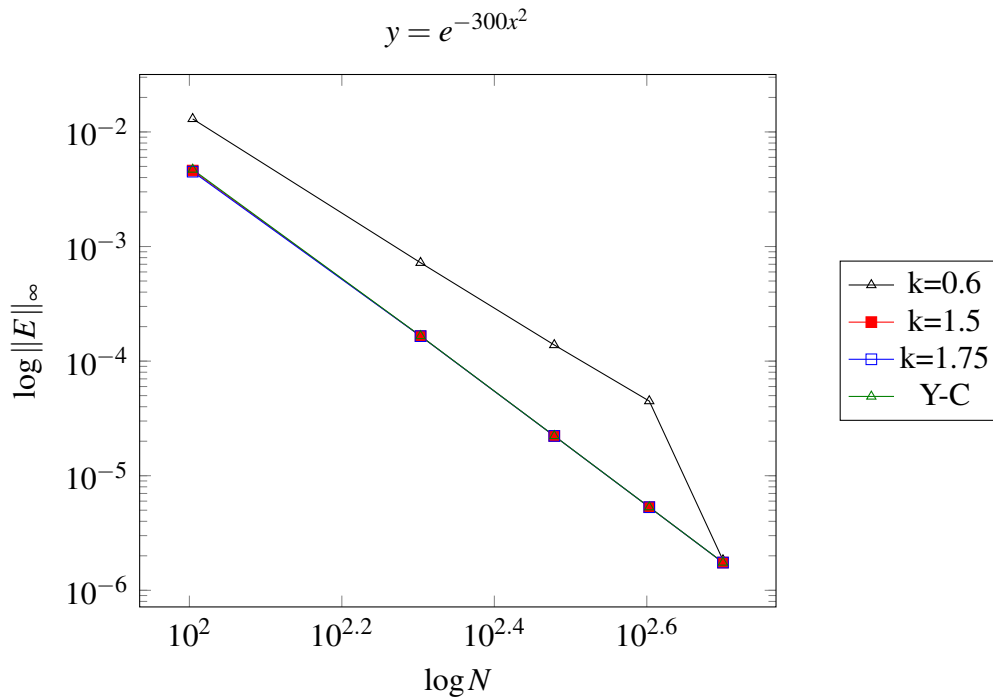


*Figure 11.* Error Convergence of 5th order ESWENO schemes with m=1.5 and selected values of k; convergent behavior for smaller values of k.

Figure 11 indicates a loss in accuracy when the value of $k$ is decreased. By significantly decreasing the stiffness of the WENO operator, we sacrifice the accuracy of the numerical scheme on coarse computational grids. This implies that making $k$ too small will result in the loss of accuracy when approximating sufficiently smooth solutions.

# CHAPTER 5

## Discussion and Future Research

Improved formulas for the weight functions of the 5th-order ESWENO scheme of Yamaleev and Carpenter were derived. For the improved weight functions, the parameters $k$ and $m$ can assume infinitely many values. Upon recognizing that there are no optimal values of these parameters, numerical tests were executed using smaller values of $k$ and $m$ to minimized the stiffness of the WENO operator. For smooth solutions, monotonic convergence at the 5th-order rate is obtained for all values of $k$ when $m = 1.5$ When $m = 1.2$, monotonic convergence at the 5th-order rate is obtained for all values of $k$ on sufficiently refined computational grids. For coarse computational grids. Accuracy is lost when $k = 1.5$. It was also demonstrated that making the value of $k$ too small results in significant losses of accuracy. For discontinuous solutions, results show that $k = 1.5$ and $m = 2$ provided the most improvement in reconstruction order near the shocks, without being overly dissipative. These same results indicate that increasing the power of $k$ results in amplification of oscillatory behavior near strong discontinuities.

Based on observations, the values $k = 1.75$ and $m = 2$ are the recommended values for the improved weight functions. Having $k = 1.75$ when $m = 2$ also provides improved reconstruction order near the shocks. The determining factor was that having $k = 1.75$ and $m = 2$ provide the design order of accuracy on both coarse and refined computational grids for sufficiently smooth solutions. Results showed that $k = 1.5$ and $m = 2$ only provided these properties on sufficiently refined computational grids. Note that the recommended values are not the only choices of the parameters, but they obtain the desired properties of significantly reduce oscillations near regions of strong discontinuities, and retention of design order accuracy for sufficiently smooth regions of the solution.

References

[1] S. Osher S. Chakravarthy A. Harten, B. Engquist. Uniformly high order non-oscillatory schemes, iii. *Journal of Computational Physics*, 71:231–303, 1987.

[2] J.M. Powers A.K. Henrick, T.D. Aslam. Mapped weighted essentially non-oscillatory schemes: Achieving optimal order near critical points. *Journal of Computational Physics*, 228:542–567, 2005.

[3] G. Scherer H.O. Kreiss. *Finite element and finite difference methods for hyperbolic partial differential equations*. Mathematical Aspects of Finite Elements in Partial Differential Equations. Academic Press, 1974.

[4] Guand-Shan Jiang and Chi-Wang Shu. Efficient implementation of weighted eno schemes. *Journal of Computational Physics*, 126:202–228, January 1996.

[5] Osher S. Chan T. Lui, X.D. Weighted essentially non-oscillatory schemes. *Journal of Computational Physics*, 115:200, 1994.

[6] Bruno Costa Wai Sun Don Rafael Borges, Monica Carmona. An improved weighted essentially non-oscillatory scheme for hyperbolic conservation laws. *Journal of Computational Physics*, 227:3191–3211, November 2007.

[7] Nail K. Yamaleev and Mark H. Carpenter. A systematic methodology for constructing high-order energy stable weno schemes. *Journal of Computational Physics*, 228:4248–4272, March 2009.

[8] Nail K. Yamaleev and Mark H. Carpenter. Third-order energy stable weno scheme. *Journal of Computational Physics*, 228:3025–3047, January 2009.